UC 34 C+D
LBL-18101
Preprint c.1

Lawrence Berkeley Laboratory
UNIVERSITY OF CALIFORNIA

RECEIVED
LAWRENCE
BERKELEY LABORATORY

DEC 19 1984

LIBRARY AND
DOCUMENTS SECTION

Submitted to Nuclear Physics

MASS DEPENDENCE OF SHELL EFFECTS AT HIGH ROTATIONAL FREQUENCIES

A.O. Macchiavelli, H. Muehry, M.A. Deleplanque,
R.M. Diamond, F.S. Stephens, E.L. Dines,
and J.E. Draper

July 1984

For Reference

Not to be taken from this room

LBL-18101
c.1

Prepared for the U.S. Department of Energy under Contract DE-AC03-76SF00098

DISCLAIMER

This document was prepared as an account of work sponsored by the United States Government. While this document is believed to contain correct information, neither the United States Government nor any agency thereof, nor the Regents of the University of California, nor any of their employees, makes any warranty, express or implied, or assumes any legal responsibility for the accuracy, completeness, or usefulness of any information, apparatus, product, or process disclosed, or represents that its use would not infringe privately owned rights. Reference herein to any specific commercial product, process, or service by its trade name, trademark, manufacturer, or otherwise, does not necessarily constitute or imply its endorsement, recommendation, or favoring by the United States Government or any agency thereof, or the Regents of the University of California. The views and opinions of authors expressed herein do not necessarily state or reflect those of the United States Government or any agency thereof or the Regents of the University of California.

LBL-18101

Mass Dependence of Shell Effects at High Rotational Frequencies

A. O. Macchiavelli,[†] H. Muehry,[††] M. A. Deleplanque, R. M. Diamond, F. S. Stephens, E. L. Dines,[†††] and J. E. Draper[†††]

Nuclear Science Division
Lawrence Berkeley Laboratory
University of California
Berkeley, California 94720

This work was supported by the Director, Office of Energy Research, Division of Nuclear Physics of the Office of High Energy and Nuclear Physics of the U.S. Department of Energy under Contract DE-AC03-76SF00098.

Permanent Addresses:

[†]Comisión Nacional de Energia Atómica, Buenos Aires, Argentina

[††]Physik Institut, Universitat Basel, Switzerland

[†††]Department of Physics, University of California, Davis, CA 95616

LBL-18101

Mass Dependence of Shell Effects at High Rotational Frequencies

A. O. Macchiavelli,[†] H. Muehry,[††] M. A. Deleplanque, R. M. Diamond, F. S. Stephens, E. L. Dines,[†††] and J. E. Draper[†††]

Nuclear Science Division
Lawrence Berkeley Laboratory
University of California
Berkeley, California 94720

ABSTRACT

The continuum γ-ray spectra from the reactions ^{40}Ar (170-185 MeV) + ^{50}Ti, ^{68}Zn, ^{82}Se, ^{100}Mo → ^{90}Zr*, ^{108}Cd*, ^{122}Te*, ^{140}Nd*, respectively have been studied by using a sum-energy technique. The evolution of the γ-ray spectra with sum energy (spin) suggests the presence of rotational motion at high spins. A method to correct for incomplete feeding was applied to the γ-ray spectra and effective moments of inertia were determined. The results indicate the appearance of a new source of angular momentum at high rotational frequencies. We interpret this as the alignment of high-j orbitals from the next major shell. Simple arguments, as well as cranked-shell-model calculations, are consistent with this picture. Data on band moments of inertia, from $E_\gamma - E_\gamma$ correlation experiments, are also in accord with our interpretation.

This work was supported by the Director, Office of Energy Research, Division of Nuclear Physics of the Office of High Energy and Nuclear Physics of the U.S. Department of Energy under Contract DE-AC03-76SF00098.

Permanent Addresses:

[†]Comisión Nacional de Energia Atómica, Buenos Aires, Argentina

[††]Physik Institut, Universitat Basel, Switzerland

[†††]Department of Physics, University of California, Davis, CA 95616

1. INTRODUCTION

Nuclei generate angular momentum essentially in two ways: single-particle motion and collective motion. The competition between these two modes is perhaps the most interesting aspect of the physics of nuclei at high-spin. With (HI, xn) reactions we are able to produce nuclei at the highest spins they can accommodate. At these spins the nucleus decays via many paths, making it impossible with present techniques to do detailed spectroscopic studies. Therefore we study the unresolved "continuum" region through average moments of inertia.

Recently we have presented a method[1]) to correct the γ-ray spectra for incomplete population. This method allowed us to determine effective moments of inertia at high rotational frequencies. The results in ^{162,166}Yb (Z = 70) and ^{160}Er (Z = 68) nuclei suggest an important contribution to the total angular momentum from aligned proton orbits from the next major shell (π $h_{9/2}$, $i_{13/2}$) that approach the Fermi surface at high rotational frequencies. Furthermore, such alignments also seem to play an important role in lighter Er nuclei[2,3]) and heavier Hf and W nuclei.[3])

Do similar shell effects occur at high-spins in other regions of the periodic table? Could we observe them by studying moments of inertia? Motivated by these questions we have undertaken the present investigation. In the next section we will discuss briefly some aspects about moments of inertia. Section 3 gives a summary of the feeding correction method. Section 4 is devoted to the experimental method, analysis and results. We interpret and discuss the results in Section 5 and present our conclusions in Section 6.

2. MOMENTS OF INERTIA

Deviations from the lowest order equation for rotational motion,

$$E = \frac{\hbar^2}{2\mathcal{J}} I(I+1) \underset{I>>1}{\cong} \frac{\hbar^2}{2\mathcal{J}} I^2 \quad , \tag{1}$$

can be inferred[4]) from the study of two types of moment of inertia: the "kinematic" $\frac{\mathcal{J}^{(1)}}{\hbar^2} = I\left(\frac{dE}{dI}\right)^{-1} = \frac{I}{\hbar\omega}$ and the "dynamic" $\frac{\mathcal{J}^{(2)}}{\hbar^2} = \left(\frac{d^2E}{dI^2}\right)^{-1} = \frac{dI}{\hbar d\omega}$. In fact, it is straightforward to show that if additional I-dependent terms appear in eq (1), $\mathcal{J}^{(1)} \neq \mathcal{J}^{(2)}$. In general these two moments of inertia could be defined for any sequence of levels; in particular there are two that occur naturally in the decay processes. If we confine ourselves to a band, where the intrinsic configuration remains unchanged, we have $\mathcal{J}^{(1)}_{band}$ † and $\mathcal{J}^{(2)}_{band}$. On the other hand a typical decay path follows a sequence of bands having different configurations. Therefore the overall change of spin with frequency defines effective moments of inertia $\frac{\mathcal{J}^{(1)}_{eff}}{\hbar^2} = \frac{I}{\hbar\omega}\Big|_{path}$ and $\frac{\mathcal{J}^{(2)}_{eff}}{\hbar^2} = \frac{dI}{\hbar d\omega}\Big|_{path}$.

An important property of $\mathcal{J}_{eff}$ is that it contains contributions from both collective and single-particle angular momenta. We can separate the <u>total</u> spin change ΔI into a part within the band ΔI_{band} and an alignment Δi. Then, from the previous definitions:

$$\frac{\Delta i}{\Delta I} = 1 - \frac{\mathcal{J}^{(2)}_{band}}{\mathcal{J}^{(2)}_{eff}} \tag{2}$$

This useful relation is schematically illustrated in fig 1.

†We note that for $\mathcal{J}^{(1)}_{band}$ knowledge of the band down to $\hbar\omega \sim 0$ is required; it is for this reason that this moment of inertia is usually impossible to obtain experimentally except for the ground-state band.

2.1 Relation to experiment

It has been realized that the rotational frequency ω is the vital quantity necessary for a systematic study of band-crossing phenomena. In turn we must be able to extract it from the experimental data. Recalling the canonical equation of motion,

$$\hbar\omega = \frac{dE}{dI} \simeq \frac{E(I+1)-E(I-1)}{2} = \frac{E_\gamma}{2} \tag{3}$$

i.e., half the γ-ray energy if the transitions are stretched quadrupole.

Gamma-ray energy correlation techniques[5]) are the appropriate tool to measure $\mathcal{J}^{(2)}_{band}$. The width of the "valley" W is determined by the difference between γ-ray energies within bands:

$$W = 2\Delta E_\gamma = 2\,\frac{dE_\gamma}{dI}\,\Delta I = 8\hbar\,\frac{d\omega}{dI} = \frac{8\hbar^2}{\mathcal{J}^{(2)}_{band}} \tag{4}$$

On the other hand, the effective moment of inertia $\mathcal{J}^{(2)}_{eff}$ is proportional to the number of stretched E2 transitions dn in a frequency interval $\hbar d\omega$,

$$\frac{dn}{\hbar d\omega} = \frac{dn}{dI}\,\frac{dI}{\hbar d\omega} = \frac{1}{2}\,\frac{\mathcal{J}^{(2)}_{eff}}{\hbar^2} \tag{5}$$

The kinematic moment of inertia $\mathcal{J}^{(1)}_{eff}$ could be obtained by associating an average γ-ray energy ($\langle E_\gamma\rangle \rightarrow \hbar\langle\omega\rangle$) with an average multiplicity ($\langle M_\gamma\rangle \rightarrow \langle I\rangle$), then $\mathcal{J}^{(1)}_{eff} = \langle I\rangle/\hbar\langle\omega\rangle$. (This is known as "the centroid method.")[6]) If $\mathcal{J}^{(2)}_{eff}$ has been determined, values for $\mathcal{J}^{(1)}_{eff}$ can be obtained by integration:

$$\mathcal{J}^{(1)}_{eff} = \frac{1}{\omega}\int_0^{\omega} \mathcal{J}^{(2)}_{eff}(\omega')d\omega' \tag{6}$$

This last expression shows that, being an integral quantity, $\mathcal{J}^{(1)}_{eff}$ is not sensitive to detailed properties.

3. THE FEEDING CORRECTION METHOD

This method has been discussed previously and we refer the reader to ref. [1,3]) for a more detailed description. However, let us review here the ideas behind it and some mathematical formulas that are useful to have at hand. As we have shown in 2.1 the height of the γ-ray spectrum is proportional to $\mathcal{J}^{(2)}_{eff}$. This is true only in the frequency region which is fully populated (typically < 0.5 MeV for rare-earth nuclei made by 170-185 MeV (^{40}Ar, xn) reactions). At the highest frequencies we must correct the spectrum for incomplete feeding in order to extract values of $\mathcal{J}^{(2)}_{eff}$. Using the notation of ref [3]) we have for the height of the spectrum:

$$h(\omega) = \frac{dn}{\hbar d\omega} = \frac{1}{2}\frac{\mathcal{J}^{(2)}_{eff}(\omega)}{\hbar^2}\int_{I(\omega)}^{\infty} K(I')dI' \tag{7}$$

where K(I) is the feeding curve.

Consider now the γ-ray spectrum associated with a similar but slightly shifted (ΔI) spin distribution:

$$h_{\Delta}(\omega) = \frac{1}{2}\frac{\mathcal{J}^{(2)}_{eff}(\omega)}{\hbar^2}\int_{I(\omega)-\Delta I}^{\infty} K(I')dI' \tag{8}$$

then

$$\Delta h(\omega) = \frac{1}{2} \frac{\mathcal{J}^{(2)}_{eff}(\omega)}{\hbar^2} K(I(\omega))\Delta I \tag{9}$$

and if $I(\omega)$ is on average a monotonic function of ω:

$$\Delta h(\omega) = \frac{1}{2} F(\omega)\Delta I \tag{10}$$

where $F(\omega)$ is the feeding curve as a function of frequency. Therefore $\mathcal{J}^{(2)}_{eff}$ could be now obtained through the "true" spectrum $H(\omega)$:

$$\frac{\mathcal{J}^{(2)}_{eff}}{\hbar^2} = 2H(\omega) = 2h(\omega) \frac{\int_0^\infty \Delta h(\omega')d\omega'}{\int_\omega^\infty \Delta h(\omega')d\omega'} \tag{11}$$

A simplified description of the method is shown in fig 2. We summarize the conditions of applicability of the method in table I.

4. EXPERIMENTAL METHOD, ANALYSIS AND RESULTS

4.1 Experimental set-up

In order to select γ-ray spectra associated with similar but shifted spin distributions we have used a technique employing successive total γ-ray energy slices (sum slices). Our sum spectrometer consisted of 2 NaI (33 cm diameter x 20 cm thick) scintillators centered on the target and ≈4 cm apart. The continuum γ-ray spectra in coincidence with the sum spectrometer were recorded in 8 (12.7 cm x 15.2 cm) NaI detectors at a distance of ~1 m from the target. This allows a clear separation of neutrons by time of flight and avoids pile-up effects. A schematic view of the arrangement is shown in fig 3. As can be

seen, the NaI detectors were clustered around 0°, 90° and 180° to obtain information on the angular distributions. Forward and backward detectors were placed symmetrically to compensate the relativistic solid-angle effects. The Ge(Li) detector (~20% efficiency), also in coincidence with the sum spectrometer, was used to monitor the products of the reactions. For more details the reader is referred again to ref [3]).

4.2 Data taking

Four different reactions were studied in the present work. They are summarized in table II, which also lists the excitation energy of the compound nucleus and the maximum spin ℓ_{fus} brought into the system for which the target and projectile will fuse (obtained from the Bass[7]) model). In the last column, the maximum angular momentum ℓ_{er} that the system can hold without fissioning or emitting α particles is estimated from the liquid-drop model.[7]) The ^{40}Ar beam was provided by the LBL 88" cyclotron. We used lead-backed targets of 0.5-1 mg/cm^2. The data were taken on magnetic tape event-by-event and subsequently analyzed off-line. Approximately 30-40 x 10^6 events were recorded for each run.

We used an ^{88}Y source to match the gains of the 8 NaI detectors, which were periodically checked during the runs. Sources of ^{24}Na, ^{60}Co, ^{88}Y and ^{207}Bi were used, before and after the experiment, to obtain absolute efficiencies, peak-to-total ratios and shape-parameter values to be used by the unfolding program which corrects for the response function of the detector.

4.3 Data analysis

We shall now summarize the steps followed in the data analysis:

i) The γ-ray spectra in coincidence with different total-energy slices are obtained by the "adding back" procedure.[8])

ii) After being unfolded and normalized to their multiplicities the spectra are combined to obtain isotropic spectra; this is done under the assumption that the angular distribution contains only a significant P_2 term, i.e. $W(\theta) = 1 + A_2P_2(\cos\theta)$.

iii) To apply the feeding correction method we need to subtract the statistical component from the data to obtain a "pure yrast-like" spectrum. A form $E_\gamma^3\exp(-E_\gamma/T)$ is assumed for the statistical component, and the temperature is determined by fitting the above expression to the exponential tail of the unfolded spectrum. Fig 4 shows an example for the $^{40}Ar + {}^{82}Se$ reaction. Temperatures of 0.55-0.65 MeV were found in the cases studied.

Angular distribution results are presented as the fraction $f(E_\gamma)$, of stretched quadrupole transitions. We assume that

$$W(\theta) = 1 + f(E_\gamma) \quad A_2^{\Delta I=2} \; P_2(\cos\theta) +$$

$$+ (1 - f(E_\gamma)) \quad A_2^{\Delta I=1} \quad P_2(\cos\theta) \qquad (12)$$

where $A_2^{\Delta I=2} = 0.378$ and $A_2^{\Delta I=1} = -0.265$ were taken from ref [9]). The fraction $f(E_\gamma)$ is obtained from the ratio $\frac{W(\theta\sim17^\circ)}{W(\theta\sim80^\circ)}$.

4.4 Results

In fig 5, we present isotropic γ-ray spectra for the reaction $^{40}Ar + {}^{82}Se$ in coincidence with different sum slices (shown in the insert). The strong correlation between the average energy of the sum slices (spin) and the maximum γ-ray energy in the yrast-bump region is evident and indicates the presence of rotational motion at the highest frequencies.

The next step is to consider the difference spectra between consecutive sum slices. This is presented in fig 6; the peaks in the low-energy region correspond to lines in ^{118}Te (which is becoming the main product of the reaction for the higher slices, as seen in the Ge(Li) spectra). These reaction-channel effects, however, do not interfere with the feeding curve of Gaussian-like shape centered at about 1.6 MeV. The energies E_{min} and E_{max} define the limits of integration in eq (11).

As mentioned in table I, in order for the method to be applicable the feeding region should be composed essentially of stretched quadrupole transitions. The results of the angular distributions shown also in fig. 6 indicate ≈100% E2 in the interval E_{min} to E_{max}. The presence of dipole transitions in the low-energy region is evident. This dipole component has been previously observed in angular correlation studies.[10]) Fortunately this component subtracts out in the difference spectra and the correction is still valid.

Two corrected spectra are shown in fig 7. They correspond to different sum slices and the maximum E_γ considered corresponds to correction factors of 4. There is a good consistency between the results, which suggests that the difference slices sample similar paths and temperatures. The moment of inertia scale is only relevant for $E_\gamma > 1.2$ MeV.

A good test of the method is presented in fig 8. The corrected spectrum for a sum slice of ~20 MeV for the $^{40}Ar + {}^{50}Ti$ reaction is compared with the uncorrected one and with the uncorrected one corresponding to a sum slice ~30 MeV. It is apparent that the corrected 20 MeV spectrum follows rather closely the uncorrected 30 MeV spectrum up to ≈2.5 MeV.

We have shown with these few examples the procedures used to obtain $\mathcal{J}^{(2)}_{eff}$. The steps followed for the other reactions are identical and we will discuss the final results in section 5.

To conclude this section let us discuss the procedure to obtain $\mathcal{J}^{(1)}_{eff}$. Due to the presence of dipole transitions we have to divide eq. (6) into two terms:

$$\frac{\mathcal{J}^{(1)}_{eff}}{\hbar^2} = \frac{I_o}{\hbar\omega} + \frac{1}{\omega}\int_{\omega_o}^{\omega} \frac{\mathcal{J}^{(2)}_{eff}}{\hbar^2} d\omega \tag{13}$$

where ω_o is determined from the condition that $f(\omega) \simeq 100\%$ for $\omega > \omega_o$, and I_o is given as:

$$I_o = \underbrace{2 \cdot \tilde{f}\, M}_{\substack{\Delta I = 2 \\ \text{component}}} + \underbrace{(1 - \tilde{f})\, M}_{\substack{\Delta I = 1 \\ \text{component}}} \tag{14}$$

Here M is the γ-ray multiplicity and $\tilde{f}$ is the average E2 fraction for $0 < E_\gamma < 2\,\hbar\omega_o$. Values of $\mathcal{J}^{(1)}_{eff}$ were also calculated by converting the multiplicity into spin by expression (14), and using the centroid method, but in this case f is averaged over all γ-ray energies.

5. DISCUSSION

At the highest frequencies all the nuclei studied appear to exhibit rotational behavior. This conclusion is based on the strong correlation observed between the average sum-energy (spin) and the maximum energy of the yrast-bump γ-transitions, and the fact that the latter are predominantly of stretched electric-quadrupole character. This transition to collective rotation at high spins was already observed in the multiplicity studies of Newton et al.,[11]) Deleplanque et al.[12]) and Aleonard et al.[13]). With the present technique of correcting the spectra for incomplete feeding, we

were able to extract values for the effective moments of inertia to high values of the rotational frequency, and hence opened the possibility of a more detailed analysis of the nuclear motion.

5.1 Effective kinematic moments of inertia, $\mathcal{J}^{(1)}_{eff}$

Let us start by discussing the results for $\mathcal{J}^{(1)}_{eff}$ that are presented in figs 9a)-d). They are rather flat, do not show any particular structure, and indicate an increase towards high ω. It is convenient to eliminate the mass dependence by scaling the results to $\frac{\mathcal{J}_{rig-sph}}{\hbar^2} = 0.0139\ A^{5/3}\ MeV^{-1}$; this is shown in fig 10. As expected, they follow closely the $A^{5/3}$ dependence, and the values are close to those of rigid-bodies, though smaller if deformation is considered. According to general arguments, $\mathcal{J}^{(1)}_{eff}$ should approach, on average, $\mathcal{J}_{rig}$ after the pairing correlations have been quenched.

5.2 Efective dynamic moments of inertia, $\mathcal{J}^{(2)}_{eff}$

The dynamic moments $\mathcal{J}^{(2)}_{eff}$ are more sensitive to local variations and we proceed now to analyze them. From fig 11a)-d) we observe a rise in the moments of inertia after a certain frequency characteristic of each system. When compared to the kinematic moments we find that $\mathcal{J}^{(2)}_{eff} \neq \mathcal{J}^{(1)}_{eff}$ and, as mentioned in section 2, this is a clear indication that the nuclei do not behave like perfect rotors. Two mechanisms come to mind: shape changes and particle alignments. These effects, however, are interrelated and, for example, it is known that the alignment of high-j particles can induce changes in deformations.

Guided by the observation[1,2]) of particle alignments from the next major shell in rare-earth nuclei, we will concentrate our discussion on this effect as the probable new source of angular momentum indicated by the rise in

$\mathcal{J}^{(2)}_{eff}$. We will try to see if, from this assumption, a consistent picture emerges. We should mention, however, that with the present data it is impossible to determine whether these alignments are accompanied by shape transitions or not. A clue on this point will be given in 5.3.

To gain more insight into the problem, consider the simplified shell model illustrated in fig 12. Influenced by the rotation, the highest j orbit from the next major shell will drop down to the Fermi surface defined by the valence shell, and cross it at a critical frequency ω_c. The slope gives the alignment,

$$\frac{\Delta\varepsilon}{\hbar\omega_c} \simeq -j \tag{15}$$

Since $\Delta\varepsilon = -\hbar\omega_0 = -41\ A^{-1/3}$ MeV and $j = N_{max} \simeq A^{1/3}$ we find a critical frequency:

$$\hbar\omega_c \simeq \frac{41\ A^{-1/3}\text{MeV}}{A^{1/3}} = 41\ A^{-2/3}\text{MeV} \quad , \tag{16}$$

which defines a "natural unit" in which to measure frequencies. This was done to the experimental data and the results are presented in fig 13.

It is surprising that all the data seem to rise at the same reduced frequency, $\omega/\omega_c \sim 0.5$. This result may be an accident because in our simplified picture we left out detailed information on the position of the Fermi surface in different nuclei. Variations in the Fermi surface will cause variations in the reduced frequency at which the high-j crossing takes place. The results for Er and Yb from ref [1]), also included in the figure, confirm this. The fact that the increase in $\mathcal{J}^{(2)}_{eff}$ seem to occur at $\omega/\omega_c < 1$ can be explained both by the spread in the shell-model levels and, more

important for deformed nuclei, the effect of deformation in bringing the high-j orbitals from the next major shell closer to the Fermi level. Both effects will cause the crossing to take place at a frequency lower than that given in eq (16).

It is difficult to make an exact assignment of the single-particle orbits involved in the crossing. However by the simple inspection of a Nilsson diagram it is possible to conclude that for A ~ 90 the occupation of $h_{11/2}$ levels (both neutrons and protons) constitutes the new source of angular momentum responsible for the increase in $\mathcal{J}^{(2)}_{eff}$. In the A ~ 108 region the effect can be associated with $\pi\ h_{11/2}$ alignments since for these nuclei $\nu\ h_{11/2}$ alignments take place at lower frequencies. In close analogy with the alignment of $i_{13/2}$ protons in Er (Z = 68),[1]) the alignment of $i_{13/2}$ neutrons in ^{118}Te (N = 66) is consistent with the observed increase in $\mathcal{J}^{(2)}_{eff}$. Finally, for ^{136}Nd it is likely that $\pi\ i_{13/2}$ and possibly $\nu\ i_{13/2}$ are large contributors to the rise in the moment of inertia.

This qualitative discussion can be supported with calculations based on the cranked-shell model.[14]) As an example, single-particle orbits for ^{118}Te in the rotating frame are shown in fig 14. A distinctive crossing is observed at $\hbar\omega$ ~ 0.78 MeV. It corresponds to the promotion of an N = 4 neutron into N = 6 ($i_{13/2}$ as mentioned previously) with an expected gain in alignment $\Delta i \simeq \langle j_x \rangle \cong 6$. Similar calculations were performed for typical nuclei produced in the different reactions and are summarized in table III. We assumed a prolate shape with ε_2 ~ 0.2 - 0.3 (somewhat arbitrary though consistent with our experimental data) and these calculations do predict the occupation of high-j levels from the next major shell in the frequency range observed in the experiments.

5.3 Band moments of inertia, $\mathcal{J}^{(2)}_{band}$

It is well known that the band moment of inertia $\mathcal{J}^{(2)}_{band}$ can be calculated microscopically by an extension of the Inglis formula:

$$\mathcal{J}^{(2)}_{band} = 2 \sum_{\substack{p\ occ \\ h\ non-occ}} \frac{\left| \langle \overset{\omega}{p} | j_x | \overset{\omega}{h} \rangle \right|^2}{e^{\omega}_p - e^{\omega}_h} \qquad (17)$$

From it we can see that a particle alignment will reduce the value of $\mathcal{J}^{(2)}_{band}$ since then j_x is diagonal and will not contribute to the sum in eq (17). If our picture is correct, we expect at the highest frequencies $\mathcal{J}^{(2)}_{band} < \mathcal{J}_{rig}$. The alignment contribution, Δi, can be obtained from eq (2) by comparing the values of $\mathcal{J}^{(2)}_{eff}$ and $\mathcal{J}^{(2)}_{band}$. The γ-γ correlations technique is still being developed, especially the background subtraction methods, and unfortunately not much data are available. However some work has been done for nuclei in the regions considered here: $^{118,122}Xe$[15]) and ^{136}Nd.[16]) In these cases it is observed that $\mathcal{J}^{(2)}_{band} \sim 0.8\,\mathcal{J}_{rig-sph}$ at the highest frequencies, $\hbar\omega \sim 0.7$ MeV. The contribution to the total change in spin (ΔI) from particle alignments (Δi) can be estimated from eq (2) to be $\frac{\Delta i}{\Delta I} \sim \frac{2}{3}$ taking a value of $\mathcal{J}^{(2)}_{eff} \sim 1.2\,\mathcal{J}_{rig-sph}$ in the same frequency range. This value of $\Delta i/\Delta I$, similar to that found in the Er, Yb systems, supports the picture of particle alignments we have been discussing.

6. CONCLUSIONS

Four different systems produced by (HI,xn) reactions in the mass region A = 90–140 were studied at high angular momentum. By using a sum spectrometer we were able to follow the spin evolution of the continuum γ-ray spectra from the decay of the evaporation residues. The strong correlation between sum-

energy slices (spin) and γ-ray energy suggests that these nuclei exhibit a quasi-rotational behavior at high rotational frequencies. The results of angular distributions indicate that the yrast-bump transitions are mainly stretched quadrupoles, hence supporting the idea of collective motion. By applying the feeding correction method, values of $\mathcal{J}^{(2)}_{eff}$ and $\mathcal{J}^{(1)}_{eff}$ were extracted for the different systems. The values of $\mathcal{J}^{(1)}_{eff}$ scale rather well with the expected $A^{5/3}$ dependence and are close to rigid-sphere values. At high frequency the increase in $\mathcal{J}^{(2)}_{eff}$ indicates the presence of a new source of angular momentum. This is interpreted as arising from the population of aligned high-j orbitals from the next major shell. This interpretation extends our previous ideas of shell effects[1,2]) to other regions of the periodic table. A rough analysis based on a simplified shell model supports this picture as do the results of cranked-shell-model calculations. Furthermore, the data suggest an $A^{-2/3}$ dependence of the frequency at which these alignments take place in agreement with the arguments given in section 5.2.

Values of $\mathcal{J}^{(2)}_{band}$ are also consistent with the particle-alignment picture: when compared with $\mathcal{J}^{(2)}_{eff}$, a ratio $\frac{\Delta i}{\Delta I} \sim \frac{2}{3}$ is obtained.

To conclude, even without resolving the γ-ray spectra, it is possible to understand the general features of the nuclear motion at high frequencies by measuring average moments of inertia. The rapid development of high-resolution multidetector arrays is pushing higher and higher the maximum spin observed, and is bringing closer the possibility of resolving the continuum. However at present, continuum γ-ray techniques are the only way to attack the problem. The present work provides the first evidence of major shell effects at very high spins over a mass range from A ~ 90-140. We believe it will serve as a guide to look for these effects with discrete γ-ray spectroscopy.

ACKNOWLEDGMENTS

One of the authors (A.O.M.) would like to thank the Lawrence Berkeley Laboratory and Comisión Nacional de Energia Atómica for financial support during his stay in Berkeley.

This work was supported by the Director, Office of Energy Research, Division of Nuclear Physics of the Office of High Energy and Nuclear Physics of the U.S. Department of Energy under Contract DE-AC03-76SF00098.

REFERENCES

(1) M. A. Deleplanque, H. J. Körner, H. Kluge, A. O. Macchiavelli, N. Bendjaballah, R. M. Diamond and F. S. Stephens Phys. Rev. Lett. 50, 409 (1983)

(2) M. A. Deleplanque, A. O. Macchiavelli, R. M. Diamond, F. S. Stephens, E. L. Dines and J. E. Draper Phys. Rev. Lett. 51, 1854 (1983)

(3) M. A. Deleplanque et al. to be published

(4) A. Bohr and B. R. Mottelson Phys. Scr. 24, 71 (1981)

(5) O. Andersen, J. D. Garrett, G. Hagemann, B. Herskind, D. L. Hillis and L. L. Riedinger Phys. Rev. Lett. 43, 687 (1979)

(6) H. J. Körner, D. L. Hillis, C. P. Roulet, P. Aguer, C. Ellegaard, D. B. Fossan, D. Habs, M. Neiman, F. S. Stephens and R. M. Diamond Phys. Rev. Lett. 43, 490 (1979)

(7) S. Cohen, F. Plasil and W. Swiatecki Ann. Phys. 82, 557 (1974), and R. Bass, Nucl. Phys. A231, 45 (1974)

(8) P. O. Tjøm, I. Espe, G. B. Hagemann, B. Herskind and D. L. Hillis Phys. Lett. 72B, 439 (1978)

(9) A. Sunyar and E. der Mateosian, Nuclear Data Tables

(10) M. A. Deleplanque, Th. Byrski, R. M. Diamond, H. Hübel, F. S. Stephens, B. Herskind and R. Bauer Phys. Rev. Lett. 41, 1105 (1978)

(11) J. O. Newton, I. Y. Lee, R. S. Simon, M. M. Aleonard, Y. El Masri, F. S. Stephens and R. M. Diamond Phys. Rev. Lett. 38, 810 (1977)

(12) M. A. Deleplanque, I. Y. Lee, F. S. Stephens, R. M. Diamond and M. M. Aleonard Phys. Rev. Lett. 40, 629 (1978)

(13) M. M. Aleonard, Y. El Masri, I. Y. Lee, F. S. Stephens, M. A. Deleplanque and R. M. Diamond Nucl. Phys. A350, 190 (1980)

(14) R. Bengtsson and S. Frauendorf Nucl. Phys. A327, 139 (1979)

(15) H. El-Samman, V. Barci, T. Bengtsson, A. Gizon, J. Gizon, L. Hildingsson, D. Jerrestom, W. Klamra, R. Kossakowski, G. A. Leander and Th. Lindblad Proceedings of the International Symposium on In Beam Spectroscopy, Hungary (1984) p. 30

(16) NBI-Berkeley Collaboration—unpublished data

TABLE CAPTIONS

I. Summary of the conditions of applicability of the feeding correction method.

II. Reactions studied in the present work. Values are given for the energy in the center of mass (E_{cm}), the excitation energy (E^*_{CN}) of the compound nucleus, the maximum angular momentum ℓ_{fus} below which the nuclei will fuse, and the maximum angular momentum ℓ_{er} the evaporation residues can hold (without fissioning or emitting alpha particles).

III. Critical frequencies extracted from the cranked shell model calculations for nuclei relevant to the present study.

TABLE I

Problem	Condition	Solution
Spin (frequency) step ΔI ($\Delta\omega$) compared to the width W	$\frac{\Delta I}{W_I}(\frac{\Delta\omega}{W_\omega}) \lesssim$ 5-10%	Proper combination of sum slices
Changing width, σ_I,* of the spin feeding curve	$\left\lvert d\sigma_I/dI_o \right\rvert < 0.2$	Minimize $d\sigma/dI$ by proper selection of sum slices
Channel effects	Should not interfere with the feeding curve	Use a high sum slice
Multipolarity of transitions	Only stretched quadrupoles in feeding region	Usually the case, at least in the nuclei studied
Frequency spread σ_ω		Effective width $\sigma = \sqrt{\sigma_I^2 + \sigma_\omega^2}$
Coherent backbend in the feeding region ($I(\omega)$ not monotonic)		No solution. But its presence may be inferred from the uncorrected spectrum where a sharp peak should be observed

* σ_I is the standard deviation

TABLE II

Reaction		E_{Lab}(MeV)	E_{CM}(MeV)	E^*_{CN}(MeV)	$\ell_{fus}(\hbar)$	$\ell_{er}(\hbar)$
^{40}Ar +	$^{50}Ti \rightarrow {}^{90}Zr$	170	94.4	93.3	60	44
	$^{68}Zn \rightarrow {}^{108}Cd$	170	107.0	91.2	63	56
	$^{82}Se \rightarrow {}^{122}Te$	170	114.3	92.0	67	64
	$^{100}Mo \rightarrow {}^{140}Nd$	185	132.1	95.1	73	65

TABLE III CRANKED-SHELL-MODEL-CALCULATIONS

Nucleus	ϵ	Protons	$\hbar\omega_c$	Neutrons	$\hbar\omega_c$
^{84}Sr	0.25	$h_{11/2}(N=5)$	1.32	$h_{11/2}(N=5)$	0.79
^{102}Pd	0.2	$h_{11/2}(N=5)$	0.75	$h_{11/2}(N=5)$	0.18[a),c)]
^{118}Te	0.25	$g_{7/2}$ (N=4)	1.0	$i_{13/2}(N=6)$	0.78
^{136}Nd	0.3	$i_{13/2}(N=6)$	0.76	$i_{13/2}(N=6)$	0.32[b),c)]

[a)] This crossing takes place in the valence shell. A backbending is observed in ^{104}Pd, ^{106}Pd at $\hbar\omega \sim 0.35$.

[b)] This crossing may occur at low frequencies; there is evidence from the observed Ge(Li) spectrum of a sharp backbending taking place at $\hbar\omega \sim 0.38$.

[c)] These values should not be considered realistic since at low frequencies pairing plays an important role in determining the values of the crossing frequencies.

FIGURE CAPTIONS

1. A typical path followed by the nucleus in its decay towards the ground state. The contributions from alignments (Δi) and collective rotation (ΔI_{band}) to the total change in spin (ΔI) are indicated.
2. Schematic illustration of the feeding correction method for a perfect rotor. On top: two sum-energy slices (N and N+1) sample two similar, but shifted, spin feeding distributions shown in the figure. From the difference between the two associated spectra (middle) we obtain a curve (bottom) close to the average of the initial spin feeding curves.
3. Top and side view of the experimental arrangement showing the geometrical disposition of the detectors. The solid angle (Ω) for the sum and NaI detectors are indicated.
4. Gamma-ray spectrum observed for the $^{40}Ar + ^{82}Se$ reaction. The statistical component of the spectrum that is subtracted to obtain the "yrast-like" transitions is shown as a dashed line. For this case the temperature T was 0.6 MeV.
5. Normalized unfolded spectra for the reaction $^{40}Ar + ^{82}Se$ in coincidence with different sum slices as shown in the insert. The sum slices are 2.5 MeV wide and are numbered starting from 0 MeV.
6. A typical difference spectrum used to generate the feeding correction factor. The integration region (E_{min}, E_{max}) for eq (11) is indicated by the arrows. The lines in the low-energy part of the spectrum belong to ^{118}Te (see text). On top, the angular distribution results are shown as the percentage of stretched quadrupole transitions.
7. Corrected spectra from different sum slices (slice 8, full line, and slice 10, dashed line). The results are plotted up to a correction factor of 4 and the moment of inertia scale is only relevant for $E_\gamma >$ 1.2 MeV.

8. A feeding-corrected spectrum (full line) corresponding to a sum slice ≈20 MeV is compared with an uncorrected spectrum (dashed) in coincidence with a higher sum slice, ≈30 MeV. (See text.) Also shown (dotted line) is the 20 MeV uncorrected spectrum.
9. Results for $\mathcal{J}^{(1)}_{eff}$ as obtained from integration of $\mathcal{J}^{(2)}_{eff}$ (eq (13)). The points are extracted from the centroid method.
10. Summary of the results for $\mathcal{J}^{(1)}_{eff}$ presented in fig 9, in units of the rigid-sphere value $\frac{\mathcal{J}_{rig-sph}}{\hbar^2} = 0.0139\ A^{5/3}\ MeV^{-1}$.
11. Results for $\mathcal{J}^{(2)}_{eff}$ observed in the different reactions.
12. Simplified shell model, illustrating how a high-j orbital from the next shell approaches the Fermi surface, λ, (valence shell) under the influence of rotation. As discussed in the text ω_c follows an $A^{-2/3}$ dependence.
13. Summary of $\mathcal{J}^{(2)}_{eff}$ values in units of $\mathcal{J}_{rig-sph}$ as a function of the reduced frequency (ω/ω_c).
14. Single-particle levels in the rotating frame for ^{118}Te. The deformation parameters used were $\epsilon_2 = 0.25$, $\epsilon_4 = 0.$, $\gamma = 0°$. Levels are indicated as follows: Positive-parity, signature = +1/2 (solid) and -1/2 (dashed), and negative parity, signature = +1/2 (dotted) and -1/2 (dot-dashed). Note the crossing at $\omega \approx 0.78$ MeV which corresponds to the population of an N = 6 ($i_{13/2}$ neutron) level.

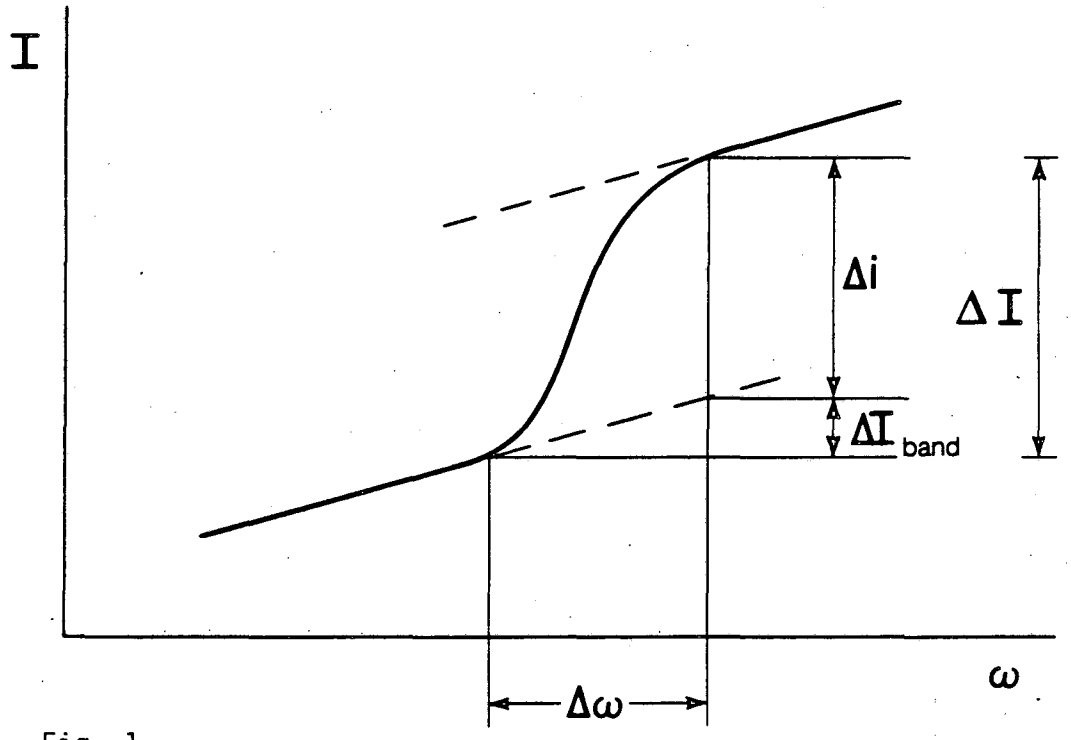

Fig. 1

XBL 847-10730

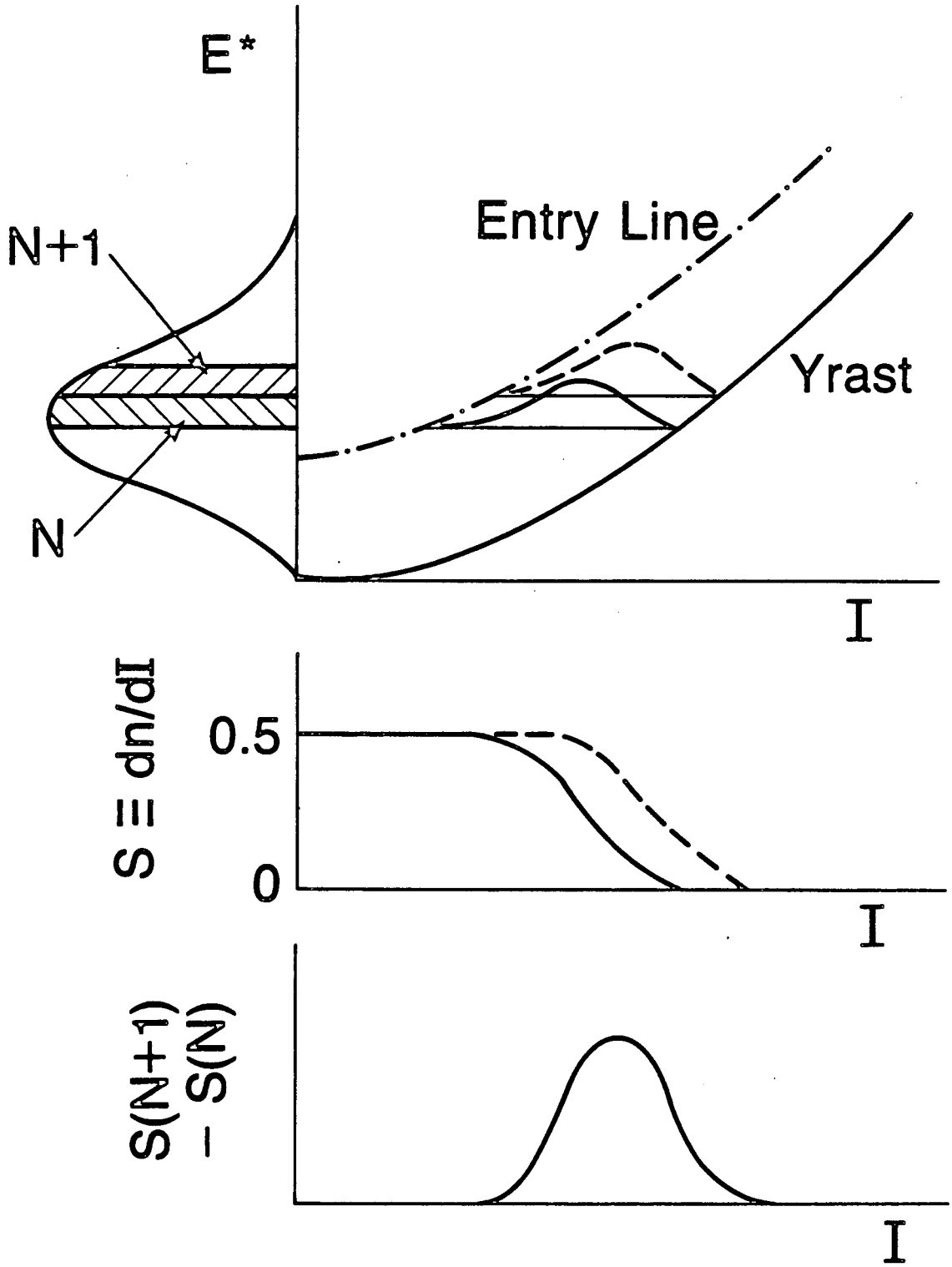

Fig. 2

XBL 847-10710

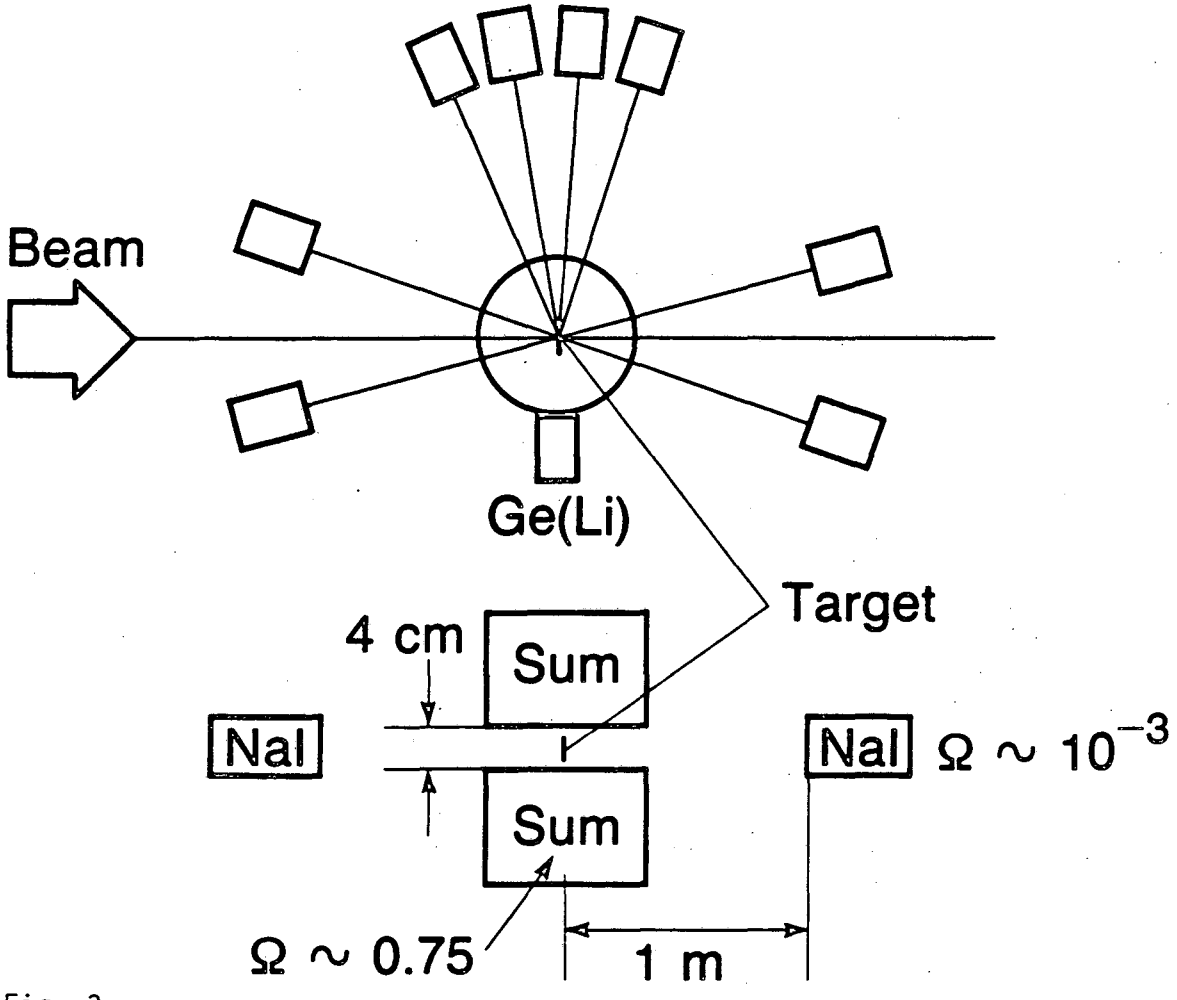

Fig. 3

XBL 848-3402

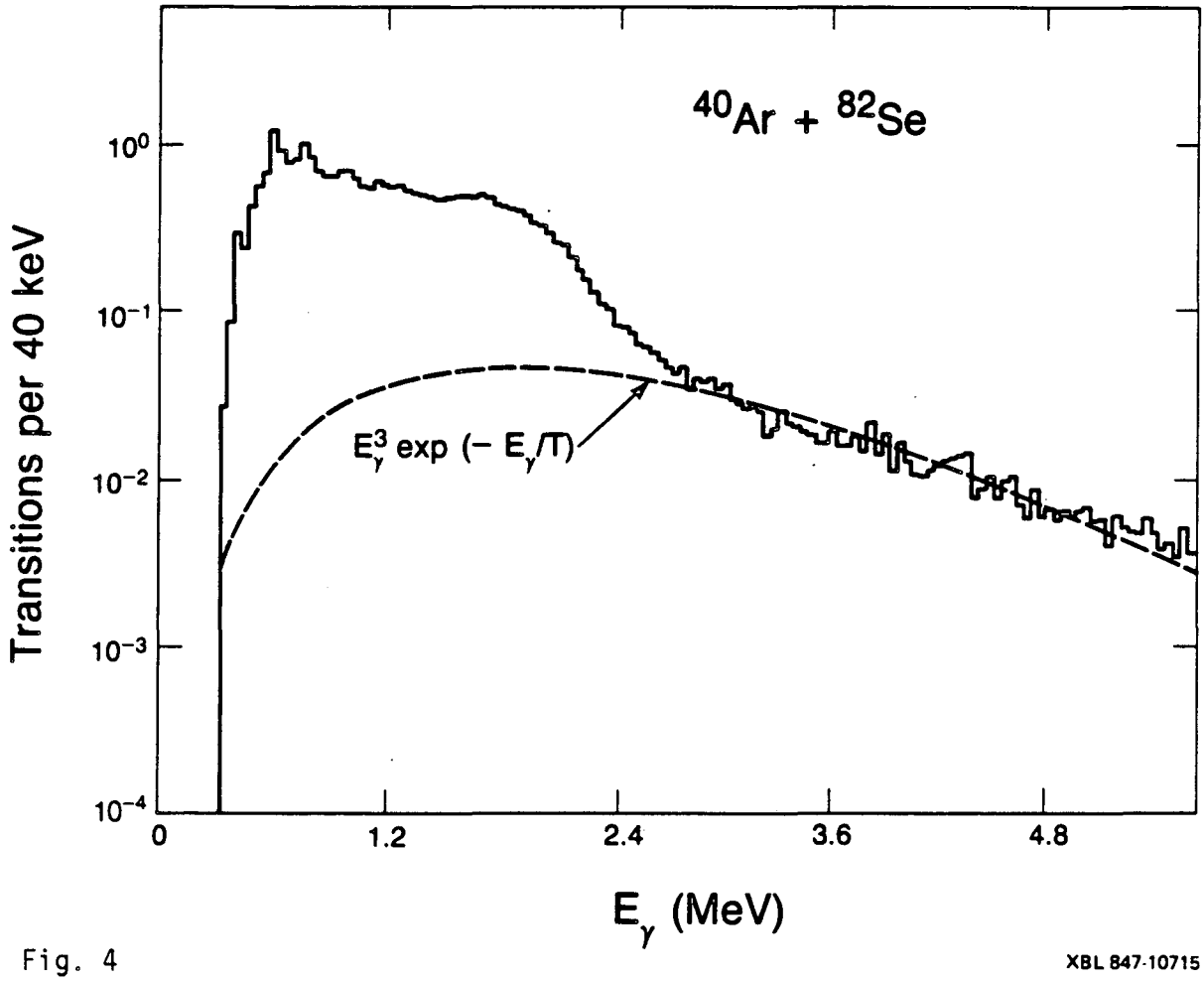

Fig. 4

XBL 847-10715

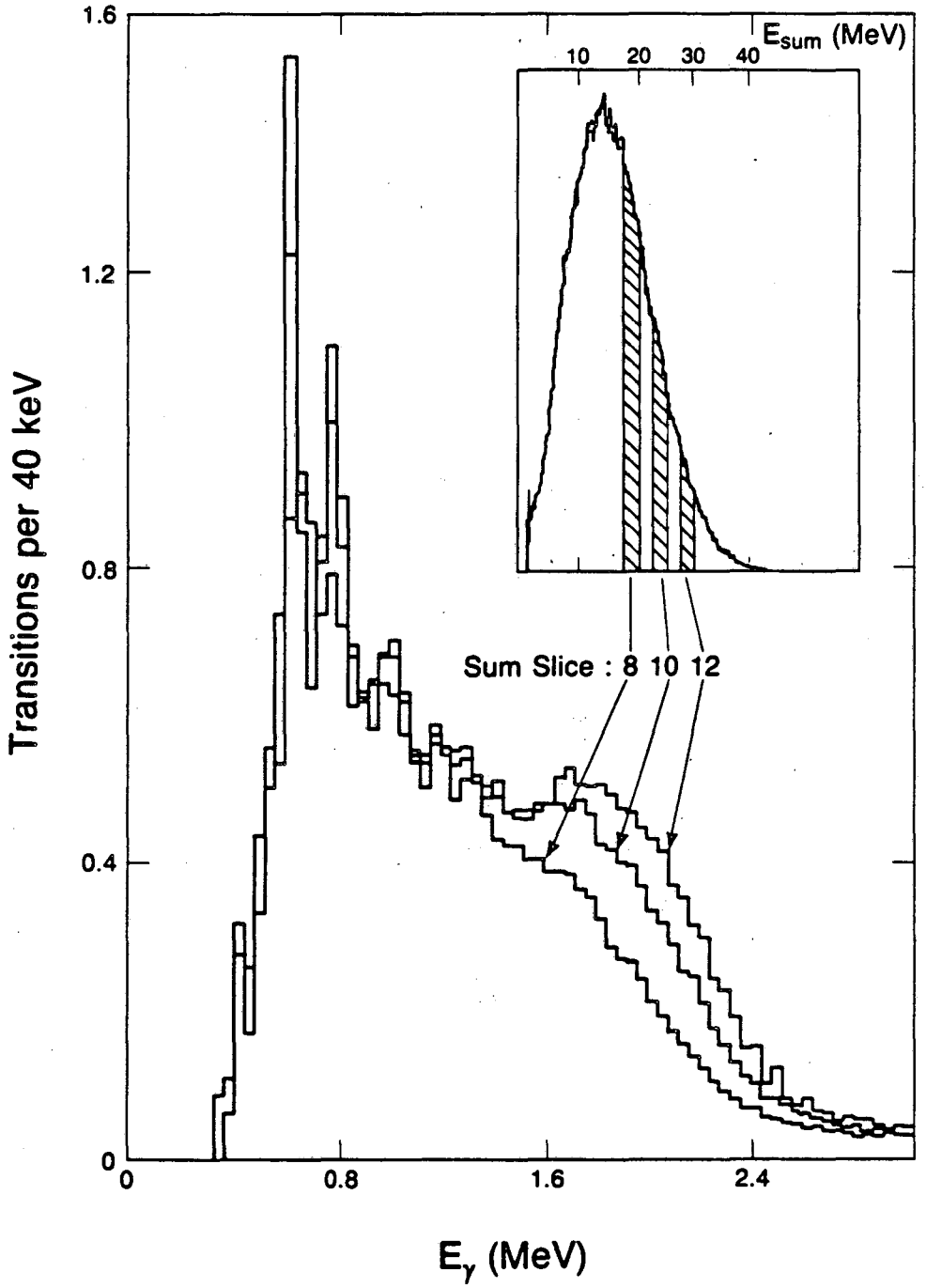

Fig. 5

XBL 847-10719

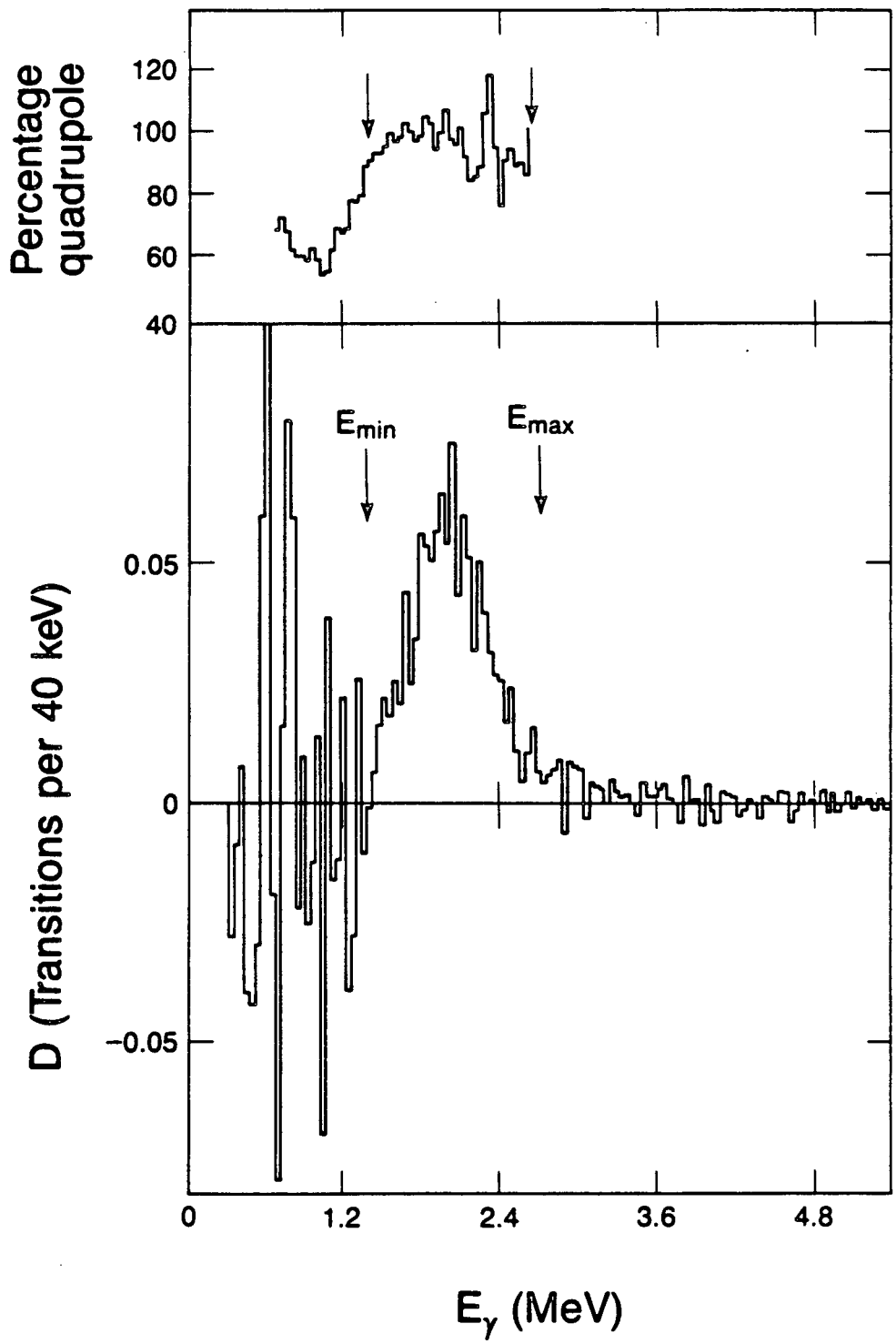

Fig. 6

XBL 847-10708

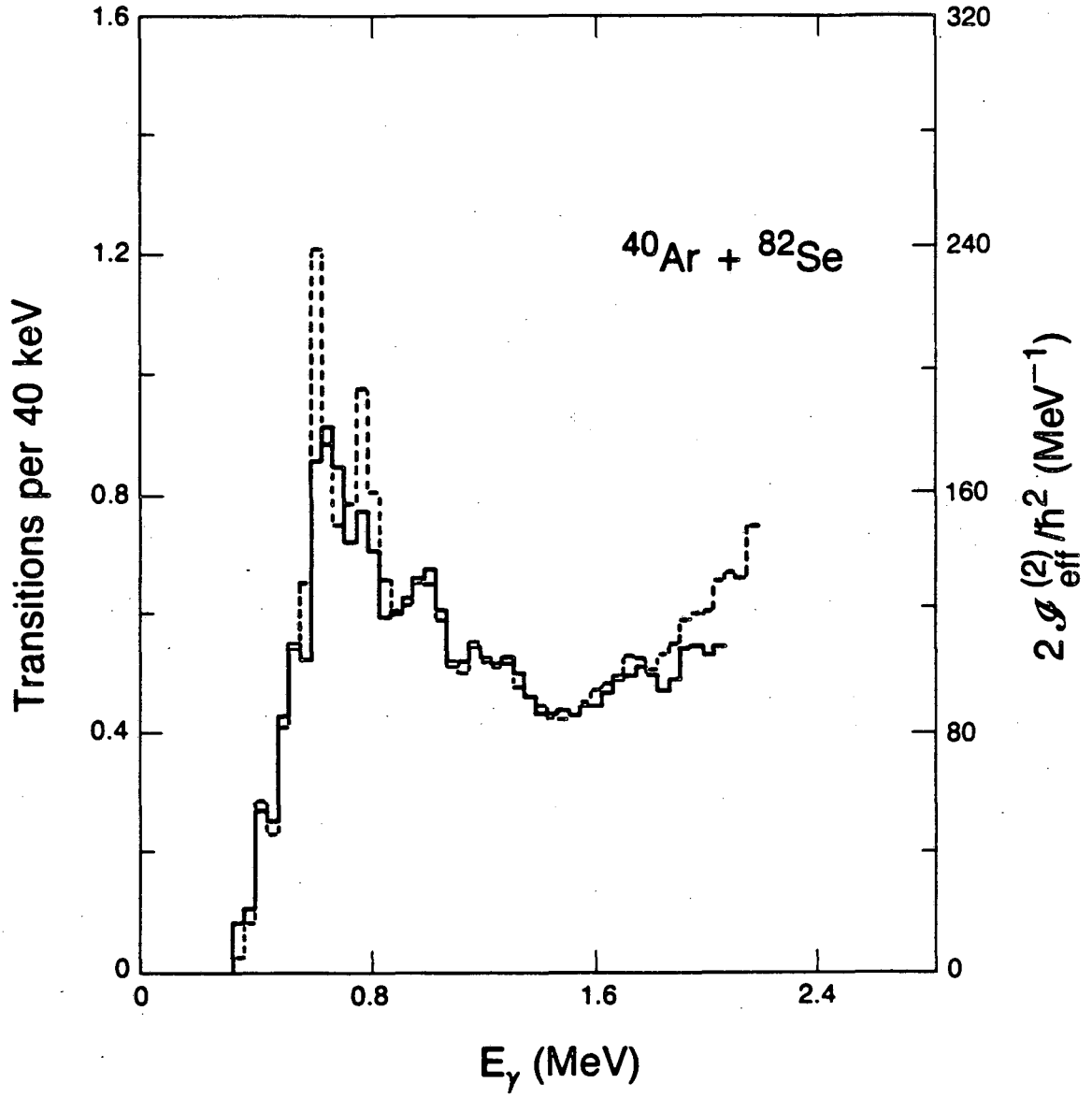

Fig. 7

XBL 847-10714

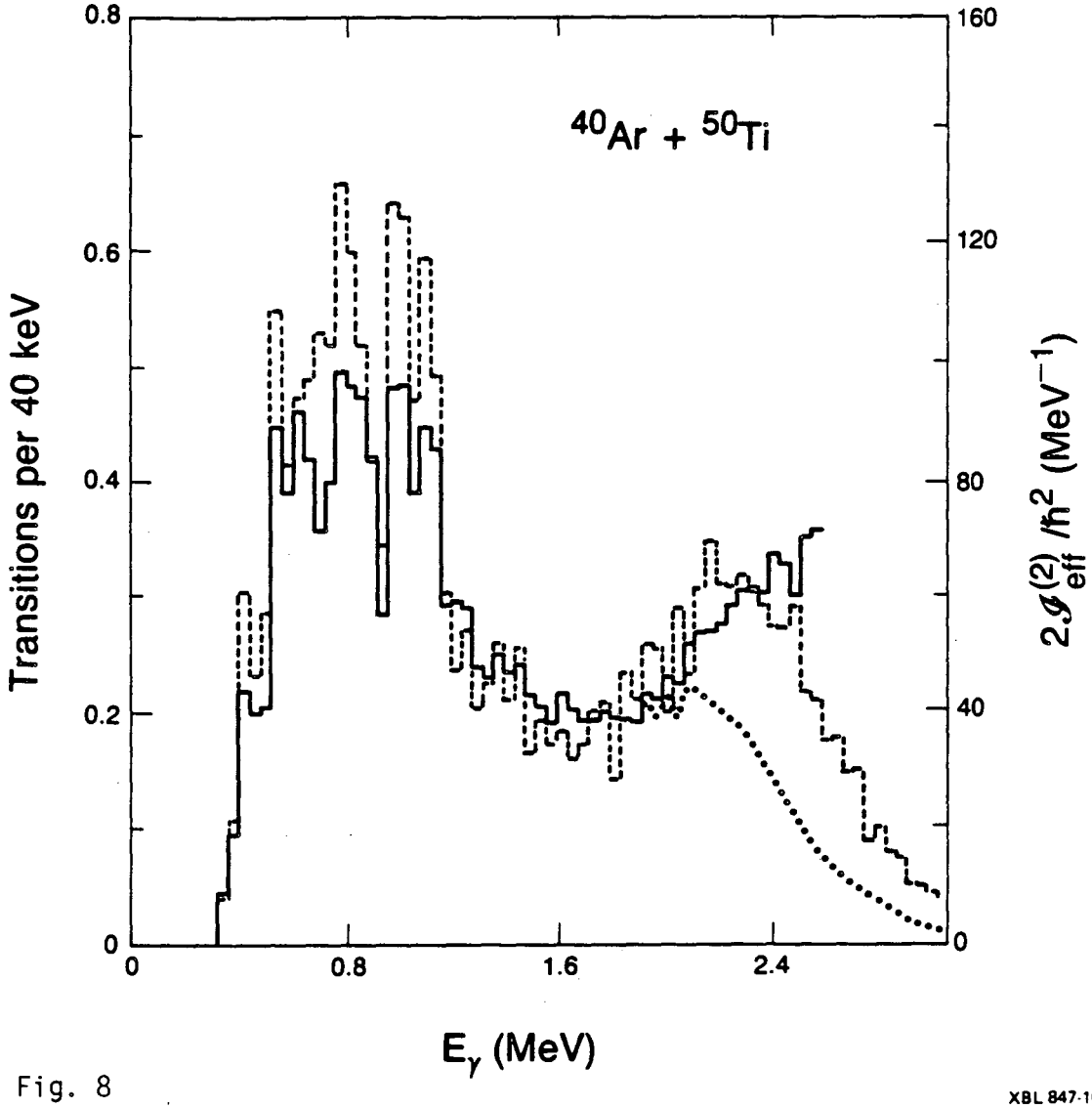

Fig. 8

XBL 847-10706

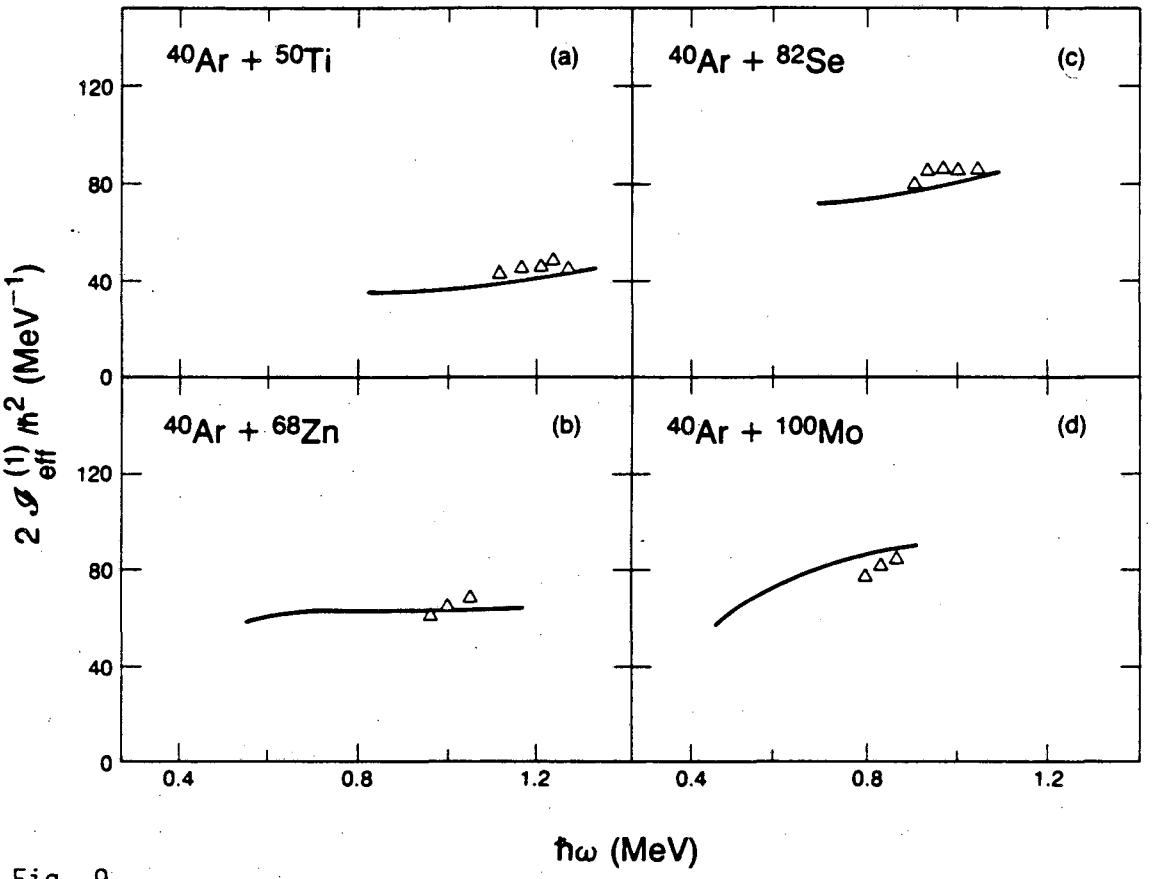

Fig. 9

XBL 847-10712

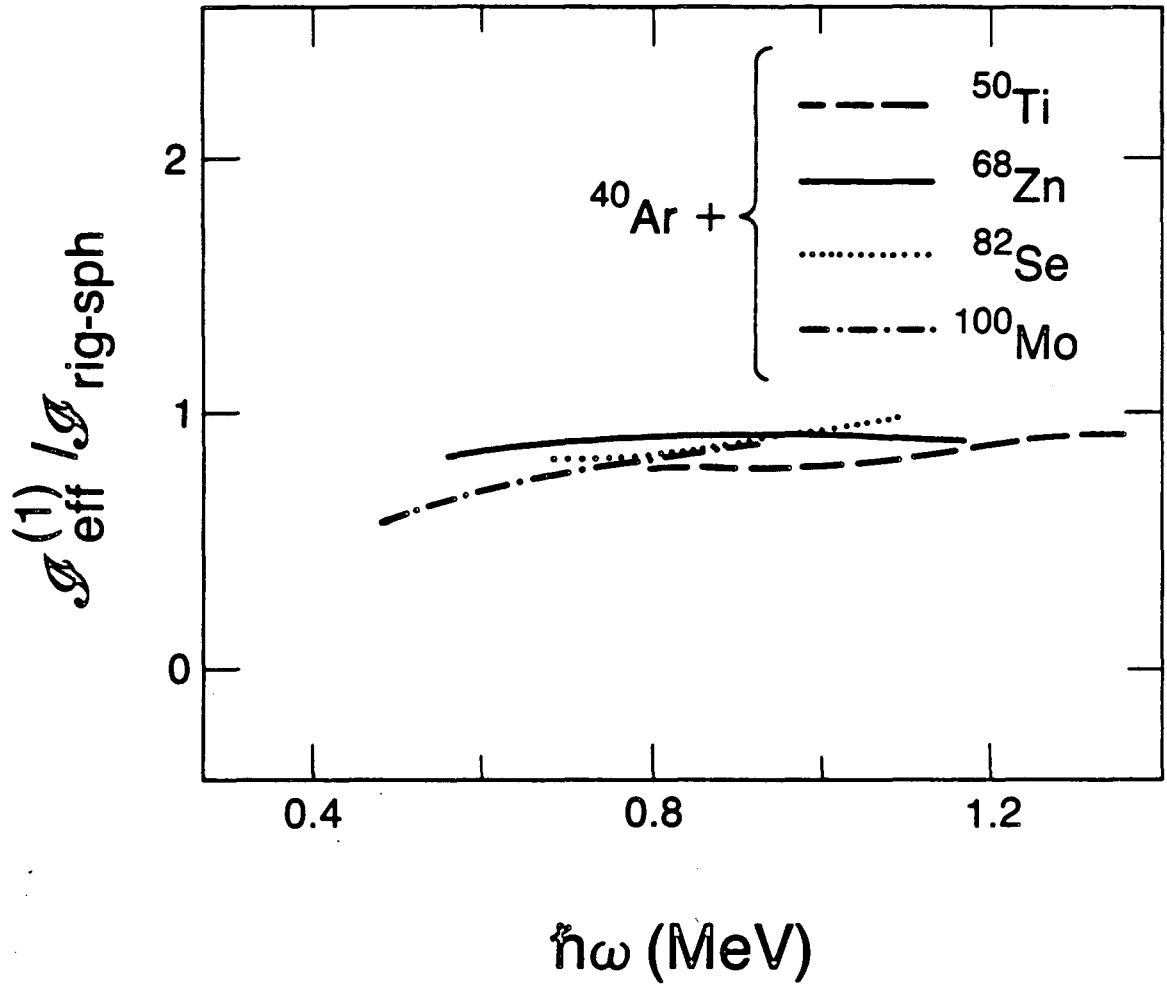

Fig. 10

XBL 847-10716

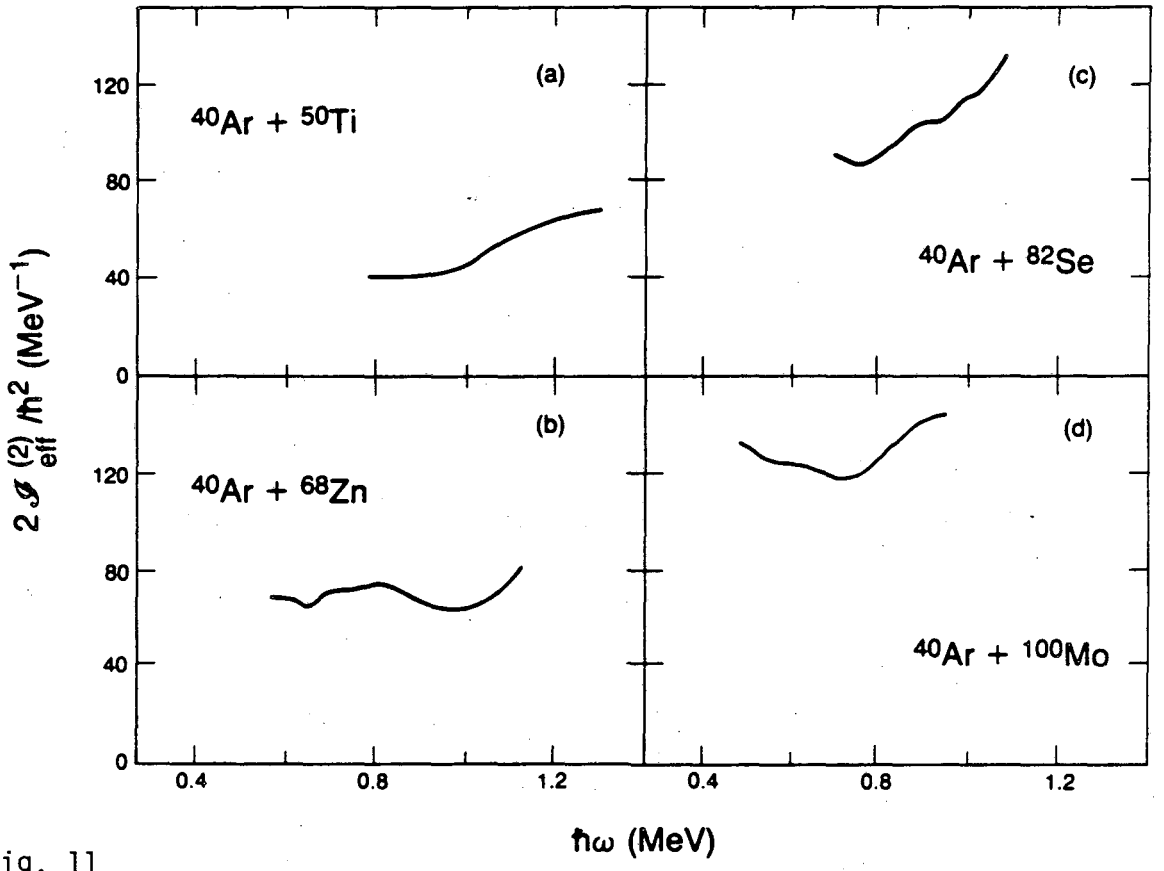

Fig. 11

XBL 847-10717

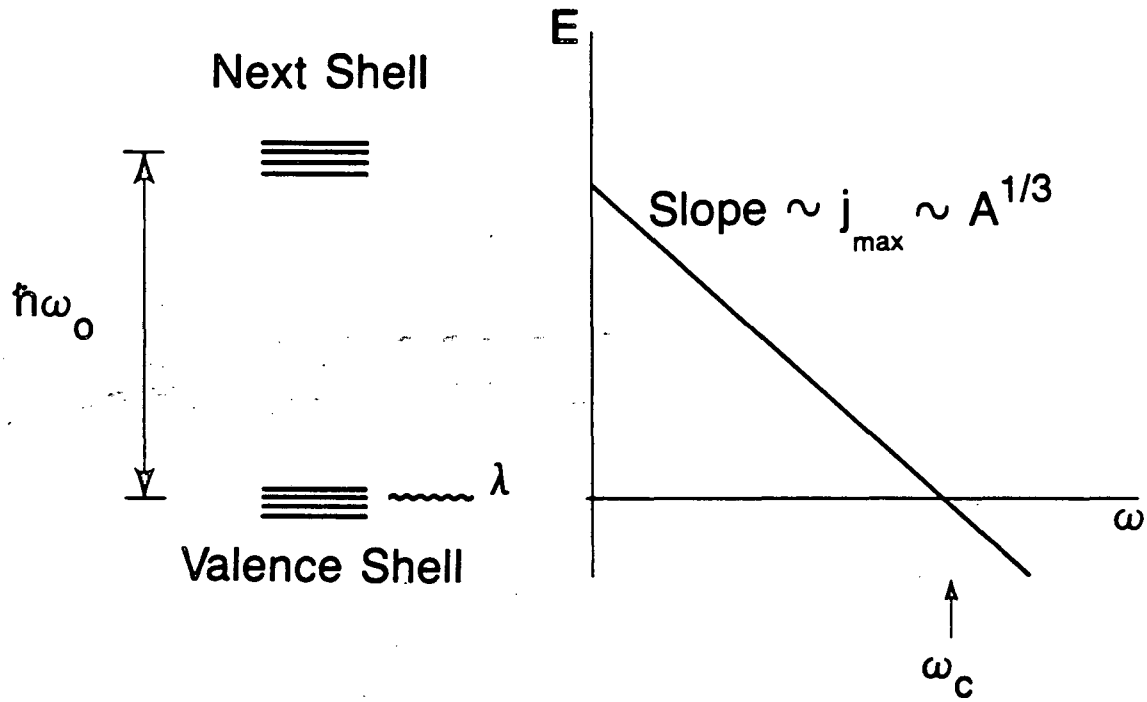

Fig. 12

XBL 847-10709

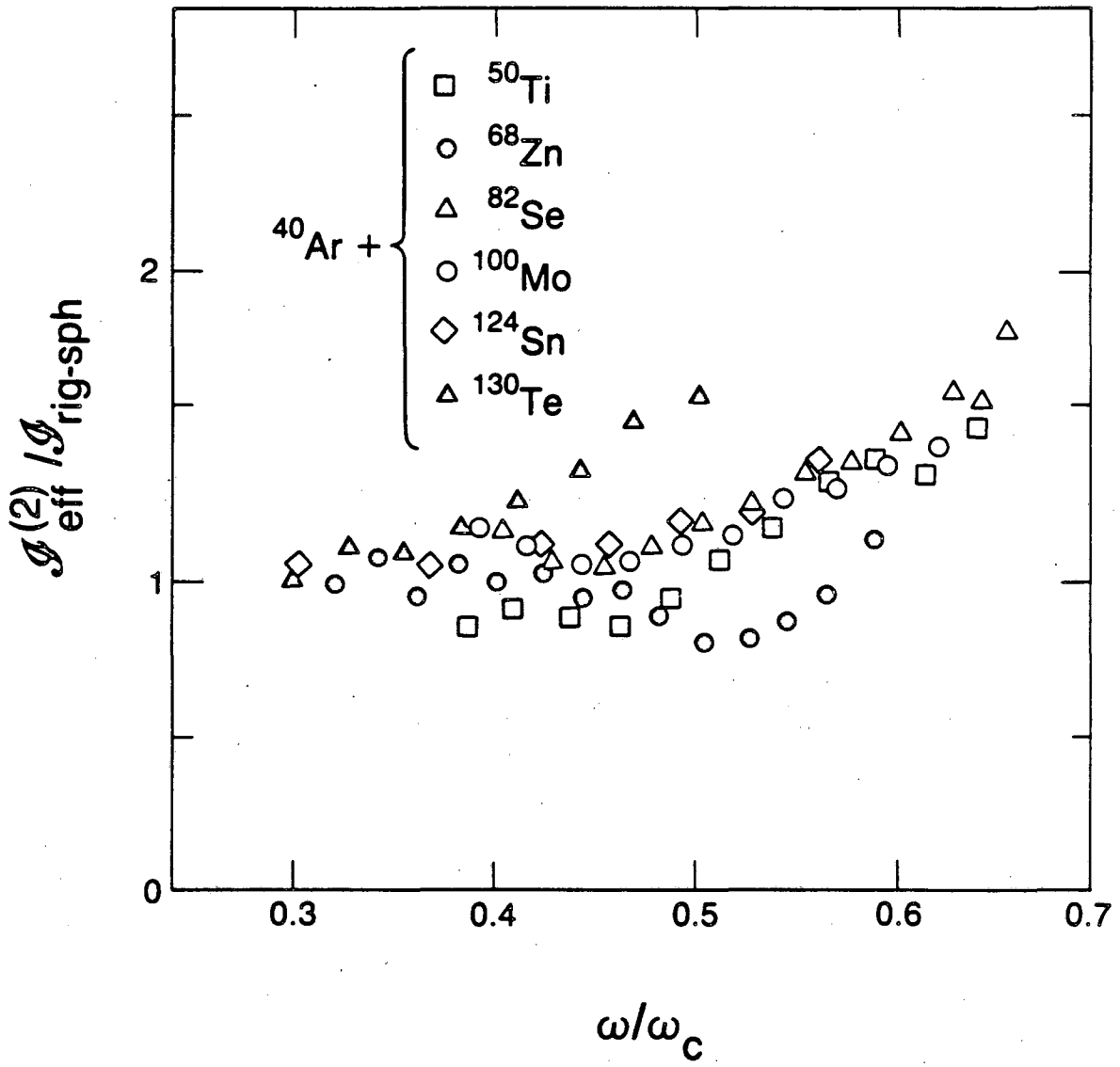

Fig. 13

XBL 847-10707

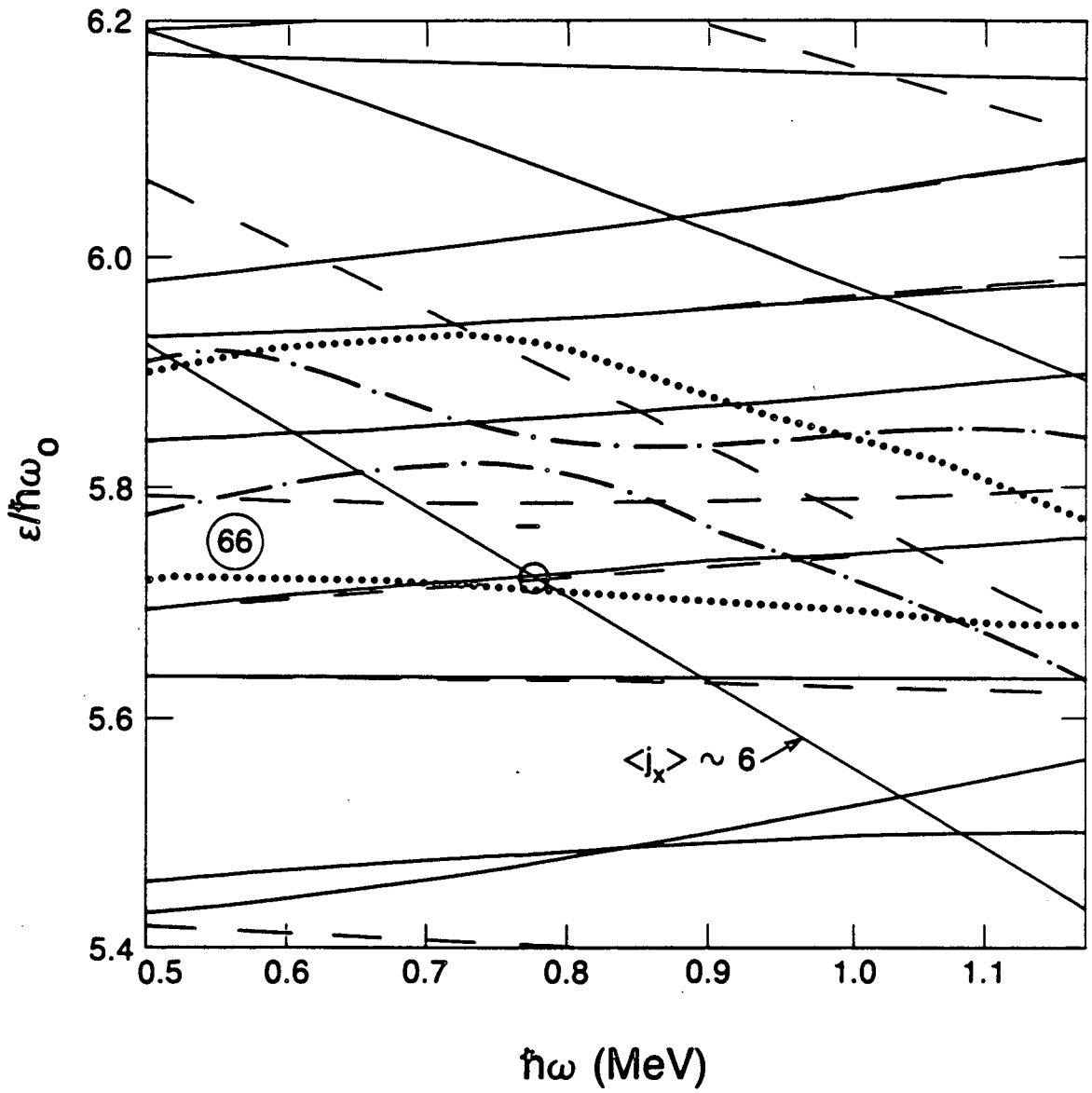

Fig. 14

XBL 847-10711

This report was done with support from the Department of Energy. Any conclusions or opinions expressed in this report represent solely those of the author(s) and not necessarily those of The Regents of the University of California, the Lawrence Berkeley Laboratory or the Department of Energy.

Reference to a company or product name does not imply approval or recommendation of the product by the University of California or the U.S. Department of Energy to the exclusion of others that may be suitable.

TECHNICAL INFORMATION DEPARTMENT
LAWRENCE BERKELEY LABORATORY
UNIVERSITY OF CALIFORNIA
BERKELEY, CALIFORNIA 94720